DSMC-SPARTA implementation of M-1 scattering model

Cite as: AIP Conference Proceedings **2132**, 070023 (2019); https://doi.org/10.1063/1.5119577
Published Online: 05 August 2019

Shashank Jaiswal, Israel B. Sebastião, and Alina A. Alexeenko

DSMC-SPARTA Implementation of M-1 Scattering Model

Shashank Jaiswal[1], Israel B. Sebastião[1] and Alina A. Alexeenko[1,a)]

[1]*School of Aeronautics & Astronautics, Purdue University, West Lafayette, IN 47907, USA*

[a)]Corresponding author: alexeenk@purdue.edu

Abstract. The direct simulation Monte Carlo (DSMC) method takes advantage of phenomenological models that can efficiently reproduce macroscopic transport and chemistry rates from elementary collisional kinetic data. As in classical kinetic theory of gases, reproduction of viscosity, thermal conductivity, and diffusion coefficients rely on the scattering dynamics that particles undergo during collisions. In this work, the still under-explored Kersch & Morokoff's (M-1) phenomenological scattering model is implemented in the DSMC-SPARTA solver. In essence, this model is a modification of the well-known variable hard/soft sphere (VHS/VSS) models for repulsive interactions to have a linear distribution of scattering angles in terms of the impact parameter. Such a feature, in general, better represents observations from quasi-classical trajectory (QCT) calculations based on ab-initio data. While the energy-dependence of M-1 collision cross-section remains the same as in VHS model, M-1 predicts more realistic diffusion coefficients that are, in general, 20% higher than those obtained with VHS scattering law. M1-model recovers Schmidt numbers (Sc) within 5% of those obtained from the Lennard-Jones (LJ) and Abrahamson (Abr) interaction models at temperatures as high as 11,000 K. A distinct feature of M-1 model is the absence of the VSS anisotropic scattering fitting parameter (α) and its applicability for large range of temperatures, and therefore demands no calibration efforts other than fitting the viscosity index (ω). In this aspect, without additional computational costs, M-1 model is potentially more suitable for conditions in which experimental diffusion-data is not available to fit the VSS parameter over a large temperature interval.

INTRODUCTION

The direct simulation Monte Carlo (DSMC) is a widely used stochastic approach for solution of the integro-differential Boltzmann equation for gas flows [1] by Monte Carlo evaluation of trajectories of N-particle systems. Drag and aero-thermal heating quantification in spacecrafts incentivized the early developments of DSMC [2]. In the present era, DSMC finds application for solving rarefied gas flow problems in high-altitude hypersonic aero-thermodynamics [3], heat and mass transfer in porous media [4], vacuum technology [5], planetary sciences [6], aerosols [7], phonon transport [8], etc.

Over sufficiently small intervals, by decoupling the molecular motion and interaction processes, DSMC first advects the particles deterministically according to their velocities, also termed as *free transport*, and then describes the collisions by statistical models with a specified interaction potential. The choice of interaction potential substantially affects the simulation fidelity and computational complexity. Early implementations of the DSMC method relied on purely repulsive hard sphere (HS) interaction model [9]. The HS model, however, deviates from experimental observations for common gases [10] due to a square-root viscosity variation with temperature. The variable hard sphere (VHS) model proposed by Bird [1] results in a more general power-law viscosity variation with temperature; and has been widely used for DSMC simulations of *single-species* gas flows due to its computational efficiency and ease of implementation. The VHS model, however, deviates from experimental observations for common *multi-species* flows [11, 12] involving diffusive transport. Later, several variations of the VHS model were proposed, including, the variable soft sphere (VSS) [12], M-1 [13], generalized soft sphere (GSS) [14], all of which belong to a class of repulsive interactions. The VSS model modifies the scattering law of the VHS model by using a scattering parameter (α) that allows reproduction of measured diffusion coefficients in addition to viscosity coefficient. M-1 model is a modification of VHS model to have a linear distribution of scattering angles in terms of the impact parameter. This modification allows M-1 to reproduce correct viscosity and diffusivity without the need of additional parameter (α). The GSS model, although general, needs additional parameters for reproducing the viscosity and diffusion coefficients. The present paper aims to quantify the differences in transport properties recovered from the VHS, VSS, and the M-1 model for a

31st International Symposium on Rarefied Gas Dynamics
AIP Conf. Proc. 2132, 070023-1–070023-11; https://doi.org/10.1063/1.5119577
Published by AIP Publishing. 978-0-7354-1874-5/$30.00

variety of flow conditions involving momentum and diffusive transport processes.

In the section that follows, we give a brief overview of the multi-species Boltzmann equation. It discusses the key ideas of the phenomenological scattering models in the process. The penultimate section presents the results and discussions on implementation of M-1 scattering models. Relevant rarefied flows involving momentum and diffusive transport have been simulated in order to verify and validate the scattering models. Concluding remarks and future work are presented in the final section.

THEORY AND BACKGROUND

Suppose we consider a mixture of n species ($n \geq 2$), each of them is represented by a number distribution function $f^{(i)}(t, x, v)$, then the multi-species Boltzmann equation is given by

$$\frac{\partial f^{(i)}}{\partial t} + v \cdot \nabla_x f^{(i)} = \sum_{j=1}^{n} Q^{(ij)}(f^{(i)}, f^{(j)}), \quad i = 1, 2, \ldots, n,$$

where $f^{(i)} = f^{(i)}(t, x, v)$ is the one-particle distribution function of time t, position x, and particle velocity v. $f^{(i)}\,\mathrm{d}x\,\mathrm{d}v$ gives the number of particles of species i to be found in an infinitesimal volume $\mathrm{d}x\,\mathrm{d}v$ centered at the point (x, v) of the phase space. $Q^{(ij)}$ is the collision operator taking into account interactions between species i and j, and acts only in the velocity space:

$$Q^{(ij)}(f^{(i)}, f^{(j)})(v) = \int_{\mathbb{R}^d} \int_{S^{d-1}} B_{ij}(|v - v_*|, \sigma \cdot \widehat{(v - v_*)}) \left[f^{(i)}(v') f^{(j)}(v'_*) - f^{(i)}(v) f^{(j)}(v_*) \right] \mathrm{d}\sigma\ \mathrm{d}v_*. \tag{1}$$

where (v, v_*) and (v', v'_*) denote the pre- and post- collision velocity pairs, σ is the vector varying over the unit sphere S^2, and B_{ij} is the collision kernel depending only on $|v - v_*|$ and angle between $v - v_*$ and σ, and $B_{ij} = B_{ji}$. During collisions, the momentum and energy are conserved

$$m_i v + m_j v_* = m_i v' + m_j v'_*, \quad m_i |v|^2 + m_j |v_*|^2 = m_i |v'|^2 + m_j |v'_*|^2, \tag{2}$$

where m_i, m_j denote the mass of particles of species i and j respectively. Then

$$\begin{cases} v' = \dfrac{m_i v + m_j v_*}{(m_i + m_j)} + \dfrac{m_j}{(m_i + m_j)} |v - v_*| \sigma, \\ v'_* = \dfrac{m_i v + m_j v_*}{(m_i + m_j)} - \dfrac{m_i}{(m_i + m_j)} |v - v_*| \sigma. \end{cases} \tag{3}$$

where $m_i v + m_j v_* / (m_i + m_j)$ is the velocity of center of mass of the pair.

The quantity B_{ij} (≥ 0) is the collision kernel depending only on $|v - v_*|$ and the scattering angle χ (angle between $v - v_*$ and $v' - v'_*$), and can be expressed as

$$B_{ij} = B_{ij}(|v - v_*|, \cos\chi), \quad \cos\chi = \frac{\sigma \cdot (v - v_*)}{|v - v_*|}. \tag{4}$$

Given the interaction potential between particles, the specific form of B_{ij} can be determined using the classical scattering theory (cf. [15]):

$$B_{ij}(|v - v_*|, \cos\chi) = |v - v_*|\, \Sigma_{ij}(|v - v_*|, \chi), \tag{5}$$

where Σ_{ij} is the differential cross-section given by

$$\Sigma_{ij}(|v - v_*|, \chi) = \frac{b_{ij}}{\sin\chi} \left| \frac{\partial b_{ij}}{\partial \chi} \right|, \tag{6}$$

with b_{ij} being the impact parameter.

With the advent of petascale computing and recent advances in applied mathematics, it is possible to solve the full Boltzmann for complex spatially non-homogeneous non-equilibrium flow problems [16, 17, 18, 19]. In practice, however, direct simulation Monte Carlo (DSMC) is a standard approach for studying rarefied non-equilibrium flows of engineering interest. Under certain assumptions, DSMC has been shown to reproduce Boltzmann kinetic equation via a Monte Carlo integration [20]. Strictly speaking, the DSMC method can be derived rigorously as the Monte Carlo solution of the N-particle master kinetic equation [21].

Scattering Models

With a few exceptions (e.g. hard sphere molecules), the explicit form of differential cross-section Σ_{ij} can be hard to obtain since b_{ij} is related to χ implicitly. To avoid this complexity, phenomenological collision kernels are often used in practice with the aim to reproduce the correct transport coefficients.

Koura et al. [12] introduced a scattering model so called as Variable Soft Sphere (VSS) by assuming an *explicit* cosine dependence between scattering angle and impact parameter, defined as:

$$\chi = 2\cos^{-1}\{(b_{ij}/d_{(ij)})^{1/\alpha_{ij}}\}, \tag{7}$$

where α_{ij} is the scattering parameter, and $d_{(ij)}$ is the diameter borrowed from Bird's (cf. equation 4.73 in [1]) Variable Hard Sphere (VHS) model, which is defined as

$$d_{(ij)} = d_{(\mathrm{ref},ij)}\left[\left(\frac{2k_B T_{(\mathrm{ref},ij)}}{\frac{m_i m_j}{m_i+m_j}|v-v_*|^2}\right)^{\omega_{ij}-0.5}\frac{1}{\Gamma(2.5-\omega_{ij})}\right]^{1/2}. \tag{8}$$

Here Γ denotes the usual Gamma function, $d_{(\mathrm{ref},ij)}$, $T_{(\mathrm{ref},ij)}$, and ω_{ij} are, respectively, the reference diameter, the reference temperature, and the viscosity index. The diameter $d_{(\mathrm{ref},ij)}$ and exponent α_{ij} are determined so that the transport (viscosity and diffusion) coefficients of VSS are consistent with experimental data.

However, the experimental diffusion-data is usually not available to fit the VSS parameter α_{ij} over a large temperature interval. Kersch [13] introduced the $M-1$ model as a modification of the well-known variable hard/soft sphere (VHS/VSS) models for repulsive interactions to have a linear distribution of scattering angles in terms of the impact parameter. The scattering in M-1 model is given as

$$\chi = \pi\{1 - b_{ij}/d_{(\mathrm{M1},ij)}\}, \quad d_{(\mathrm{M1},ij)} = \sqrt{\frac{4}{3}}d_{(ij)} \tag{9}$$

M-1 model needs only the viscosity exponent to match the experimental data on viscosity and reproduce diffusion coefficients that agree with the corresponding Schmidt numbers. It is worth noting that this linear relationship of scattering angle and the impact parameter is similar to the one obtained for high energy Lennard Jones interactions (see equation 30 in [22]). This, in part, explains why M-1 recovers Schmidt numbers (Sc) within 5% of those obtained from the Lennard-Jones (LJ) at temperatures as high as 11,000 K.

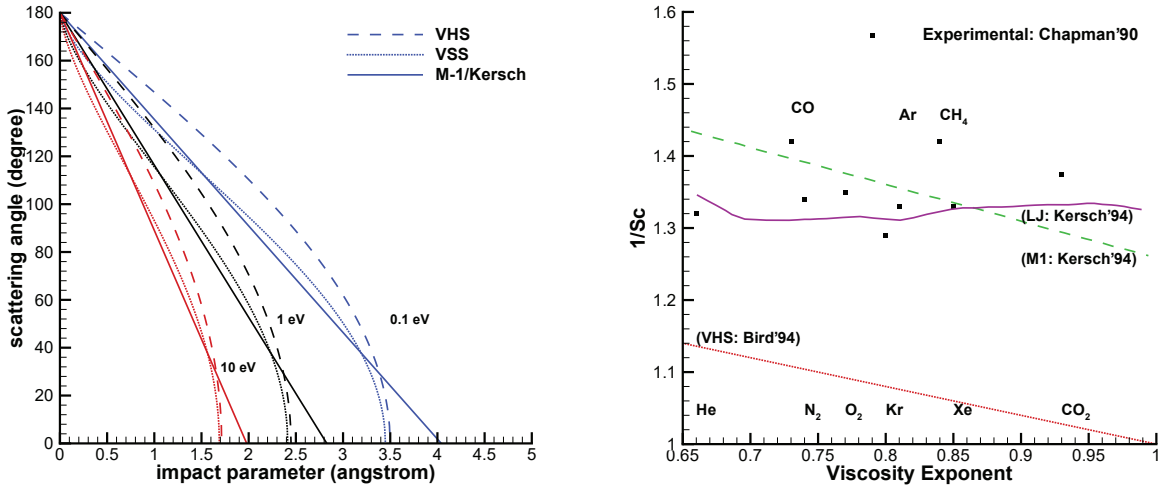

(a) (b)

FIGURE 1: (a) Variation of scattering angle *wrt* impact parameter for different scattering models at different relative collisional energies, and (b) Comparison of inverse Schmidt from different scattering models for different species against experimental data from [23].

Figure (1a) illustrates the variation of scattering angle as a function of impact parameter for VHS, VSS, and M-1 models for different relative collisional energies. M-1 model reproduces Abrahamson (Born-Mayer type) potential for high energy collisions, which is known to be near-linear for repulsive interactions [13]. This linear scattering feature, in general, better represents observations from quasi-classical trajectory (QCT) calculations based on ab-initio data.

Figure (1b) shows the inverse Schmidt number for different species. M1-model recovers Schmidt numbers (Sc) within 5% of those obtained from the Lennard-Jones (LJ) and Abrahamson (Abr) interaction models at temperatures as high as 11,000 K. While the energy dependence of M-1 collision cross-section remains the same as in VHS model, M-1 predicts more realistic diffusion coefficients that are 20% higher than those obtained with VHS scattering law. A distinct feature of M-1 model is the absence of the VSS anisotropic scattering fitting parameter (α) and its applicability for large range of temperatures.

RESULTS AND DISCUSSIONS

In this section, we verify and validate the accuracy of the M-1 model for recovering the viscosity, diffusion, and inverse Schmidt number for a range of physical conditions, including, high speed, and high temperature flows involving momentum, heat, and diffusive transport.

Standard test cases of Couette flow [24, 25], planar Ar-Ar self diffusion [1], Ar-He mass diffusion [1], and unsteady diffusion [26] have been considered in the present work. The results are compared with published experimental results, DSMC solutions, or analytical solutions wherever applicable.

SPARTA [27] has been employed for implementing M-1 model, and carrying out DSMC verifications in the present work. It implements the DSMC method as proposed by Bird [1]. Herein, given the temperature range of interest, only translational and rotational energy modes are considered. The solver has been benchmarked [27] and widely used for studying hypersonic, subsonic and thermal [17, 28, 29, 30, 31] gas flow problems. In particular, SPARTA relying on C++ object oriented design, has been shown to perform very well on massively parallel architectures [27, 28]. In this work, cell size less than $\lambda/3$ has been ensured in all the test cases. A minimum of 30 DSMC simulator particles per cell are used in conjunction with the no-time collision (NTC) algorithm. Each steady-state simulation has been averaged for a minimum 100,000 samples, which are taken at every time step, so as to minimize the statistical noise. The VHS/VSS model parameters for different species have been directly taken from [1].

Couette Flow

Couette flow serves as a test case for reproducing the correct viscosity coefficient. The coordinates are chosen such that the walls are parallel to the y direction and x is the direction perpendicular to the walls. The geometry as well as boundary conditions are shown in Figure 2. The two parallel walls are set $H = 1$m apart. The left wall is at rest, and the right wall moves in $+y$ direction. The case parameters [24, 25] have been indicated in Table (1). The simulation is carried out for three different cases corresponding to wall temperatures of 273K, 40K, and 1000K respectively. Argon is taken as the working gas.

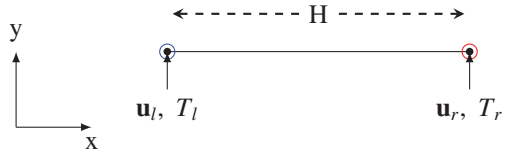

FIGURE 2: Numerical setup for Couette flow. Distance between the walls is fixed as $H = 1\,m$. $\mathbf{u}_l$, and $\mathbf{u}_r$ refer to the velocity of left and right walls respectively; whereas T_l and T_r refer to the temperature of the left and right walls respectively. The left most node of the domain has been indicated by blue, and the right most node in red.

Figure (3a) illustrates the variation of normalized temperature obtained using the Lennard-Jones Polynomial Approximation (LJPA) [24, 25], VHS, VSS, and M-1 model. The agreement between the four models is excellent with the maximum difference in normalized temperature below 0.1%. Similarly, Figures (3b, 3c, 3d) depict the difference between DSMC flow velocity and incompressible Couette flow velocity $v_{inc} = v_w\ x/H$ for three cases. At $T_w = 273K$ (Case 01), the results from all the models are comparable. For $T_w = 40K$ (Case 02), and $T_w = 1000K$ (Case 03) we

TABLE 1: Case parameters for the Couette flow [24, 25].

Quantity	Value
Initial number density, n (m^{-3})	1.4×10^{20}
Moving Wall velocity, v_w (m/s)	300
Timestep, Δt (μs)	1
Number of cells	500
Particles per cell	200
Number of transient timesteps	1.2×10^6
Number of steady timesteps	50×10^6
Molecular parameters	
Molecular mass, m_0 $(\times 10^{27}\, kg)$	66.3
Viscosity index, ω_{ij}	0.81
Scattering parameter, α_{ij}	1.4
Reference diameter, $d_{\text{ref},ij}$ $(\times 10^{10} m)$	4.17
Reference temperature, $T_{\text{ref},ij}$ (K)	273
Reference viscosity, $\mu_{\text{ref},ij}$ $(\text{Pa} \cdot s)$	2.117×10^{-5}

observe that VHS, VSS, M-1 models reproduce approximately same velocity. This conclusively asserts that all the three models reproduce the same viscosity coefficient.

Fick's Ar-Ar Self Diffusion

In the current test case, we consider the effect of diffusive transport (see section 12.5 in [1]). The schematic remains the same as in the previous test case. Argon-Argon mixture is taken as the working gas. To differentiate between two types of Argon, we tag the molecules as Ar_1 and Ar_2. At the left boundary, Ar_1 enters and exits at the right boundary. At the right boundary, Ar_2 enters and exits at the left boundary. The molecules enter the domain with zero mean velocity. The initial, and reference temperatures are kept at 273K. The schematic of the problem has been illustrated in Fig. (4).

Figure (5a) shows the variation of species concentrations along the domain using VHS, VSS, and M-1 collision models. Since the species-1 enters from the left boundary and exits at right, we observe a drop in species-1 concentration as we move towards the right boundary. Conversely for species-2, since the species-2 enters from the right boundary and exits at left, we observe a drop in species-2 concentration as we move towards the left boundary. It is also worth noting that throughout the domain at any given x location, the sum of the concentrations of two species is unity. Moreover, the concentrations from all the three models are in excellent agreement with each other.

Figure (5b) shows the variation of diffusion velocity along the domain. Since the species-1 enters from the left boundary and exits at right, we observe a low net diffusion speed for the first species and a high diffusion speed for the second species. Conversely at the right boundary, since the species-2 enters from the right boundary and exits at left, we observe a low diffusion speed for the second species and high diffusion speed for the first species. It is evident that VHS model reproduces lower diffusion speed for both species. Nevertheless, the diffusion speed from VSS and M-1 models are in excellent agreement with each other.

Fick's Ar-He Mass Diffusion

In the current test case, we consider the effect of mass diffusion for dissimilar species. The conditions remain the same as in previous case, except that Argon-Helium mixture is taken as the working gas. More specifically, Argon enters the left boundary and exits at the right boundary; and Helium enters through the right and exits at left. The schematic of the problem has been illustrated in Fig. (6).

Figure (7a) shows the variation of concentration profile for the two species. We first note that the concentrations from all the three models are in excellent agreement with each other. Next, we observe that the concentration of Helium remains greater than Argon for a larger portion of the domain. This can be directly inferred from the mass/momentum

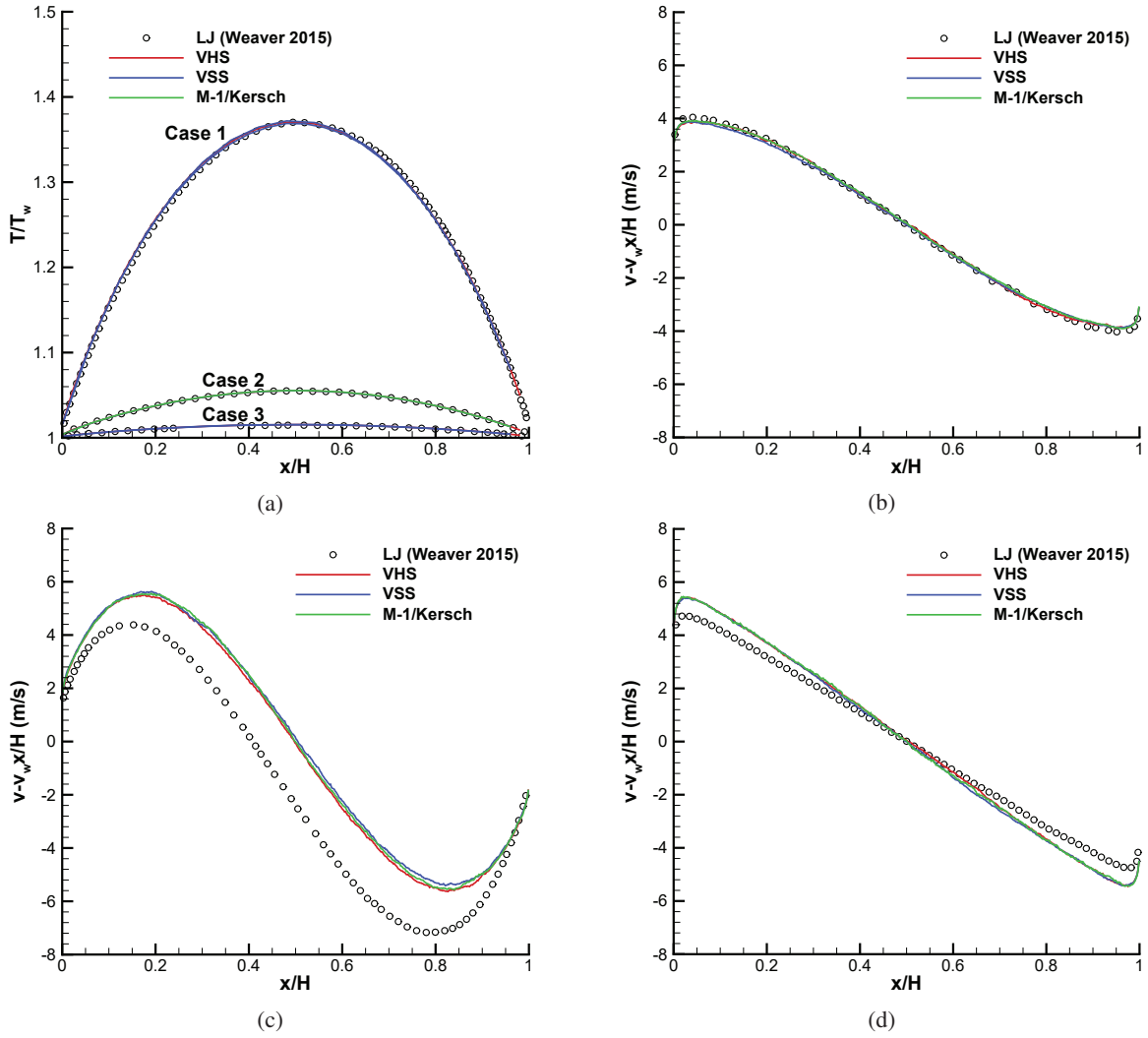

FIGURE 3: Comparison of (a) normalized temperatures for Cases 1–3, (b) velocity variation for Case 1, (c) velocity variation for Case 2, and (d) velocity variation for Case 3, along the domain length obtained using LJPA, VHS, VSS, and M-1 models.

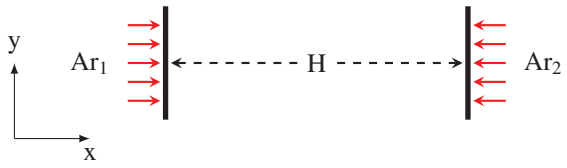

FIGURE 4: Numerical setup for Ar-Ar self diffusion. Distance between the walls is fixed as H.

conservation principle i.e., the heavier species diffuses slower and the lighter species diffuses faster. Therefore, after a sufficiently long time, the concentration of lighter species will be greater than that of heavier species for a major part of the domain. As in the self-diffusion case, the sum of the concentrations of both species is unity throughout the domain at any given x location. The effect of the momentum conservation is more pronounced in the Fig. (7b) where we observe a higher diffusion speed for the lighter species and a lower diffusion speed for the heavier species. It is again evident that VHS model reproduces lower diffusion speed for both species. Nevertheless, the diffusion speed

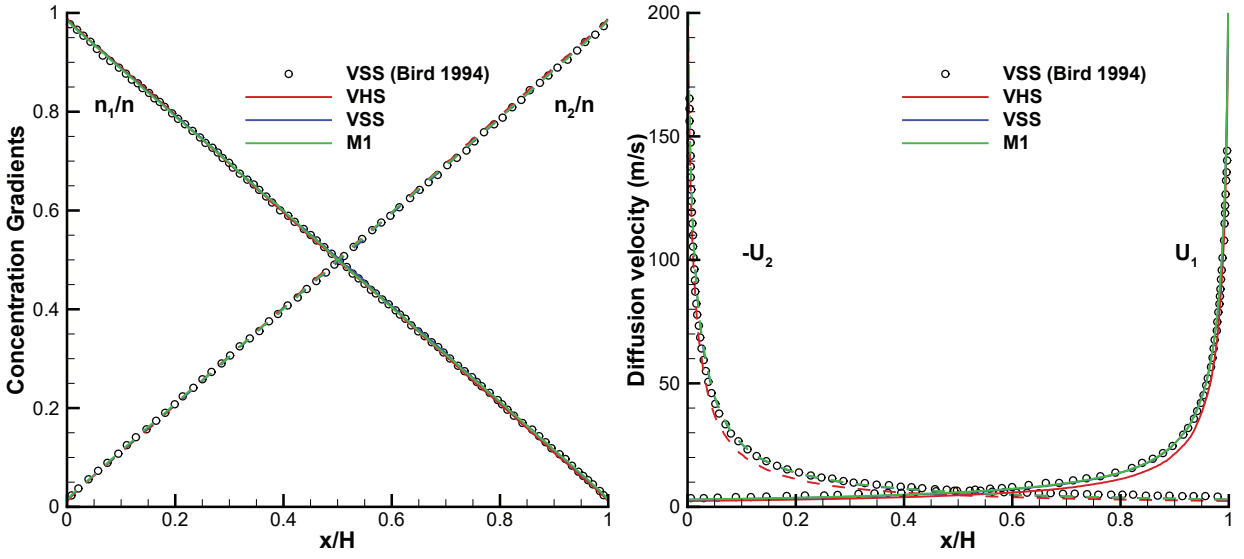

(a) (b)

FIGURE 5: Variation of number density and diffusion velocity along the domain obtained with different DSMC scattering models for Argon-Argon self-diffusion test case.

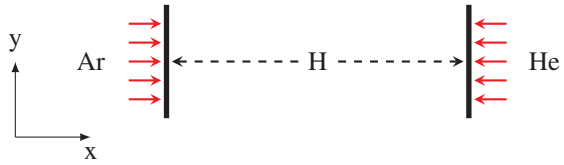

FIGURE 6: Numerical setup for Ar-He self diffusion. Distance between the walls is fixed as H.

from VSS and M-1 models are in excellent agreement with each other.

Unsteady Ar-Ar Self Diffusion

In the present simulations, we test the scattering models for reproducing analytical diffusion coefficients. This is essentially an initial value problem (see [26]). Initially at $t = 0$, the first Argon species Ar_1 is concentrated in the region $[-H, H]$, and Ar_2 occupies the rest of the domain i.e., $\{[-L, L] - [-H, H]\}$, where $L \gg H$. The schematic of the problem has been illustrated in the Fig. (8a). The initial mixture is then left to diffuse over time. The analytical evolution of concentration of first species is given as

$$\frac{C}{C_0} = \frac{1}{2}\left\{ \text{erf}\,\frac{H-x}{2\sqrt{Dt}} + \text{erf}\,\frac{H+x}{2\sqrt{Dt}} \right\} \tag{10}$$

where C is the concentration, C_0 is initial concentration, D is diffusion coefficient.

Figures (8b,9a,9b) illustrate the variation of concentration of first species along the domain at different time instants obtained from different scattering models for different temperatures. It is evident that diffusion reproduced by M-1 matches well with VSS at temperatures as high as 10000 K. At a given time instant, the diffusion reproduced by VHS model is lower than VSS and M-1.

Schmidt number

In DSMC, the phenomenological scattering models are calibrated against experimental data so that the simulation models reproduce the correct transport properties, namely, viscosity and diffusion. In the present case, we run a set of

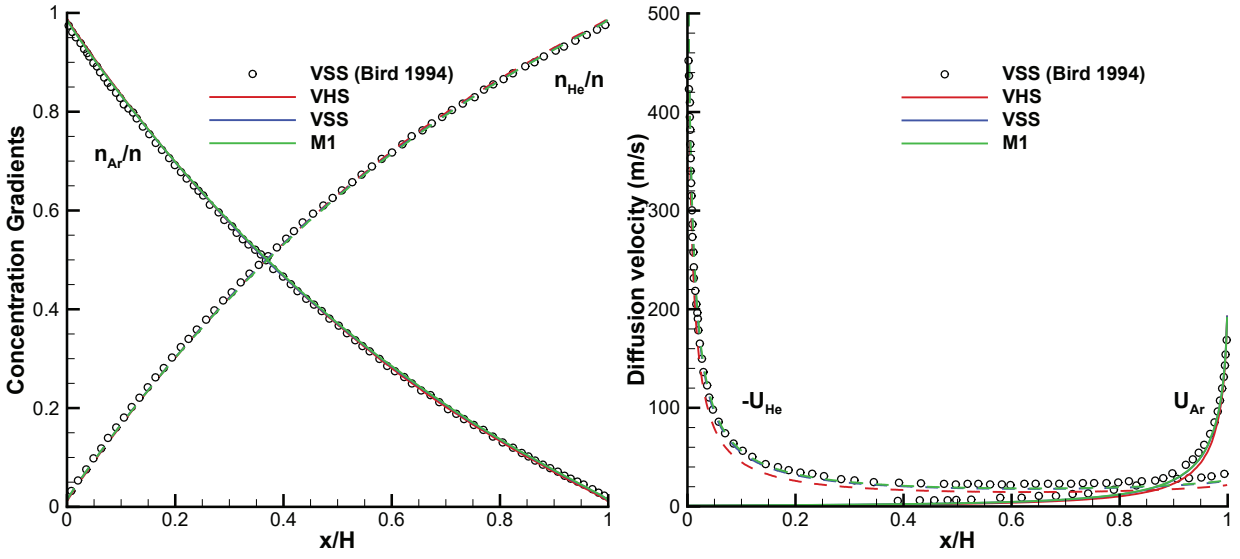

(a) (b)

FIGURE 7: Variation of number density and diffusion velocity along the domain obtained with different DSMC scattering models for Argon-Helium mass-diffusion test case.

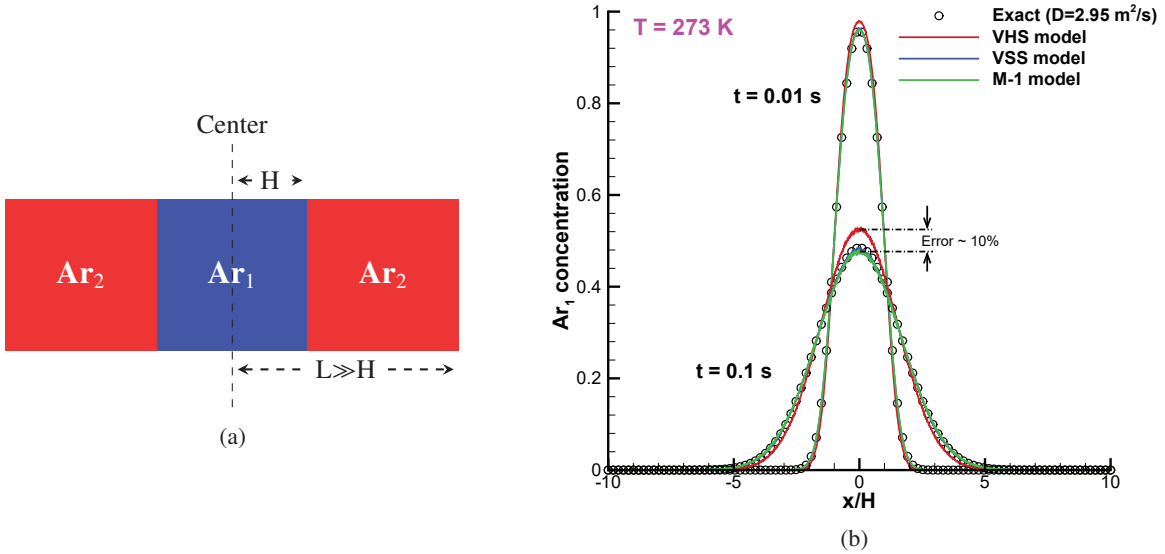

(a) (b)

FIGURE 8: (a) Schematic for unsteady Ar-Ar self diffusion test case, and (b) Variation of concentration of first species along the domain at different time instants with T=273 K.

1-D Couette and Fickian flows for extracting viscosity and diffusivity for different molecular species.

The viscosity μ is recovered from 1-D Couette flow DSMC simulations through its relationship to shear-stress and velocity-gradient relationship [25]

$$\mu = \frac{\tau}{\mathrm{d}v/\mathrm{d}x} = \frac{< \rho\, c_x\, c_y >}{\mathrm{d}v/\mathrm{d}x} \tag{11}$$

where $\mathbf{c} = \{c_x, c_y, c_z\}$ is the thermal velocity, v is y-component of velocity, τ is shear-stress, and ρ is density. The brackets, $< \ldots >$, in the expression for shear-stress denote an average value. The reported average viscosity and

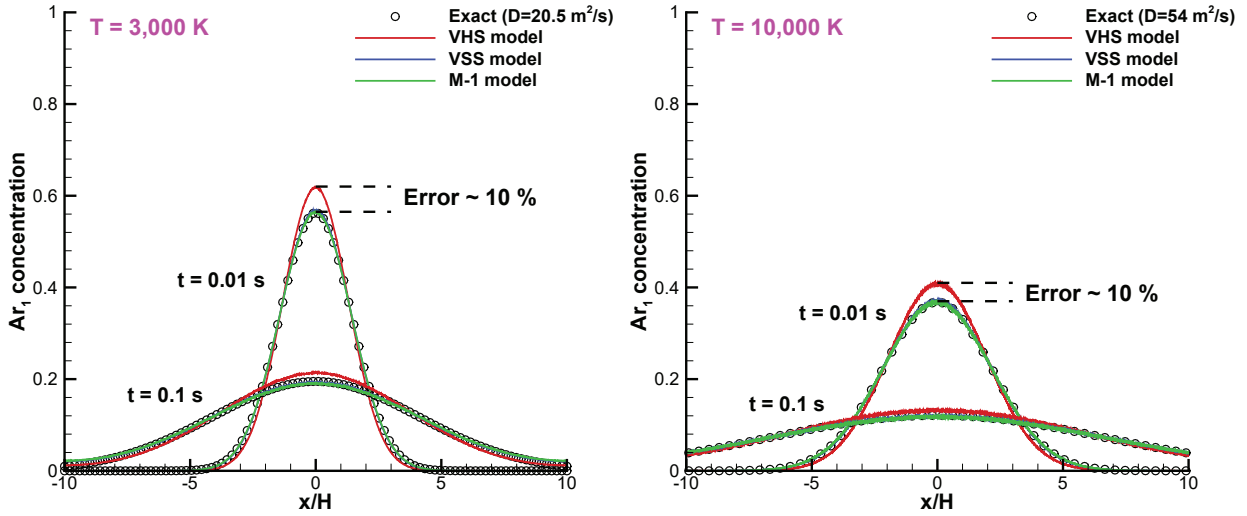

FIGURE 9: Variation of concentration of first species along the domain at different time instants in the unsteady Ar-Ar diffusion problem: (a) T=3000 K, and (b) T=10000 K

shear stress values are averaged over the central 60% of the domain. This averaging procedure is used in order to exclude possible effects of the Knudsen layer, which might extend several mean free paths from the walls.

The self-diffusion coefficient D is recovered from 1-D Fickian flow simulations using (cf. equation 12.18 in [1])

$$D = -(u_x^{(1)} - u_x^{(2)}) \frac{n^{(1)}\, n^{(2)}}{n^2} \frac{\Delta x}{\Delta(n^{(1)}/n)} \tag{12}$$

where $n^{(1)}$, $n^{(2)}$, n denote the number density of first species, second species, and the mixture respectively; and $u_x^{(1)}$, $u_x^{(2)}$ denote the x-velocity of first and second species respectively. Note that this equation is a first order approximation to the diffusion equation (see [23]), and therefore the values computed from this equation might not be entirely accurate especially for the rarefied flows, since the higher order terms have not been accounted for. It is worth emphasizing that the full diffusion equation based on moment of the distribution function is highly non-trivial from a computation perspective (see [23]). For consistency and fair comparison, we use (12) for all the models. Knowing the viscosity and diffusion coefficients, we compute the inverse Schmidt number ($\mathrm{Sc}^{-1} = \rho\, D/\mu$) from VHS, VSS, and M-1 models for different species.

Table (2) presents the viscosity, diffusivity, and inverse Schmidt numbers recovered from experiments, VHS, VSS, and M-1 models for different molecular species. Considering the error of transport property calibration (see [32]), and the statistical noise in DSMC simulations, one can infer that the M-1 model reproduces the correct viscosity and diffusivity similar to the one reproduced by VSS model, albeit without the need for extra scattering parameter α.

Figure (10) presents the inverse Schmidt recovered using different scattering models for different molecular species. The numerically recovered inverse Schmidt number is somewhat lower than the experimentally determined Schmidt number for all the models, which can be attributed to statistical/averaging errors inherent to DSMC simulations. To conclude, the M1-model recovers Schmidt numbers (Sc) within 1% (except for Helium) of those obtained from VSS model, and within 5% of those obtained from the experiments.

CONCLUSIONS

We have presented an implementation of M-1 scattering model in general purpose SPARTA-DSMC framework. M-1 model is a modification of the well-known variable hard/soft sphere (VHS/VSS) models for repulsive interactions to have a linear distribution of scattering angles in terms of the impact parameter. A distinct feature of M-1 model is the absence of the VSS anisotropic scattering fitting parameter (α) and its applicability for large range of temperatures. To

TABLE 2: Numerically determined inverse Schmidt number for various species using VHS, VSS, and M-1 models. The experimental data is taken from Chapman et al. [23].

species	μ_{exp} ($\times 10^5$ Pa $\cdot$ s)	$\frac{\mu_{vhs}}{\mu_{exp}}$	$\frac{\mu_{vss}}{\mu_{exp}}$	$\frac{\mu_{M1}}{\mu_{exp}}$	D_{exp} ($\times 10^5$ m^2/s)	$\frac{D_{vhs}}{D_{exp}}$	$\frac{D_{vss}}{D_{exp}}$	$\frac{D_{M1}}{D_{exp}}$	Sc_{exp}^{-1}	$\frac{Sc_{vhs}^{-1}}{Sc_{exp}^{-1}}$	$\frac{Sc_{vss}^{-1}}{Sc_{exp}^{-1}}$	$\frac{Sc_{M1}^{-1}}{Sc_{exp}^{-1}}$
He	1.97	0.89	0.93	0.88	15.5	0.74	0.86	0.93	1.30	0.86	0.96	1.18
CH_4	1.02	1.0	0.95	0.94	2.06	0.69	0.92	0.87	1.44	0.68	0.95	0.92
CO	1.63	0.96	1.05	0.99	1.90	0.74	0.95	0.9	1.45	0.76	0.89	0.91
N_2	1.66	1.00	1.00	1.01	1.78	0.80	0.96	0.99	1.34	0.79	0.95	0.97
O_2	1.92	1.01	1.03	1.02	1.81	0.78	0.96	0.97	1.34	0.77	0.91	0.94
Ar	2.12	1.05	1.05	1.03	1.57	0.78	0.96	0.98	1.32	0.72	0.90	0.93
CO_2	1.38	1.05	1.05	0.99	0.96	0.72	0.96	0.89	1.37	0.67	0.89	0.88
Kr	2.33	1.0	1.10	1.11	0.79	0.80	0.94	1.01	1.27	0.70	0.83	0.88
Xe	2.11	1.6	1.17	1.14	0.48	0.75	0.93	0.94	1.33	0.61	0.76	0.78
Average	–	0.92	0.93	0.91	–	0.68	0.84	0.84	–	0.73	0.89	0.93

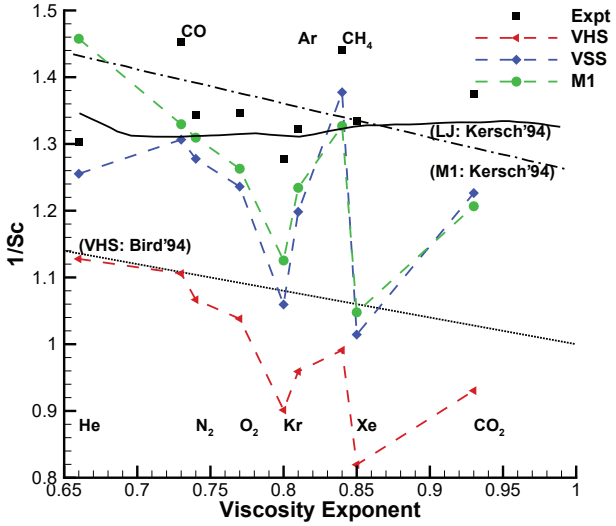

FIGURE 10: Comparison of observed inverse Schmidt from different scattering models for different species against experimental data from [23], and theoretical inverse Schmidt number.

verify the M-1 model and its implementation, we carried out rarefied-to-continuum gas flow simulations for Couette flow, planar Ar-Ar self diffusion, Ar-He mass diffusion, and unsteady diffusion flows at different Knudsen numbers and wide range of physical conditions, including, large temperatures, and large velocity gradients. Each of these cases, involving either momentum or diffusive transport, have been run with different scattering models namely VHS, VHS, and M-1. M1-model recovers Schmidt numbers (Sc) within 1% of those obtained from VSS model, and within 5% of those obtained from the experimental data. We conclude that the results obtained from M-1 and VSS are fairly close ignoring the statistical noise and the errors therein. The M-1 model, in particular, is suitable for conditions in which experimental diffusion data is not available to fit the VSS scattering parameter over a large temperature interval. The future work will likely focus on further tests for hyper-thermal velocity cases. Application for reactive flow involving multiple species is yet another interesting direction.

REFERENCES

[1] G. A. Bird, *Molecular Gas Dynamics and the Direct Simulation of Gas Flows* (Clarendon Press, Oxford, 1994).

[2] G. Bird, "Simulation of multi-dimensional and chemically reacting flows (past space shuttle orbiter)," in *Proceedings of 11th Rarefied Gas Dynamics symposium* (1979), pp. 365–388.

[3] M. Ivanov and S. Gimelshein, Annual Review of Fluid Mechanics **30**, 469–505 (1998).

[4] L. De Socio and L. Marino, Journal of Fluid Mechanics **557**, 119–133 (2006).

[5] A. Venkattraman and A. A. Alexeenko, Journal of Vacuum Science & Technology A: Vacuum, Surfaces, and Films **28**, 916–924 (2010).

[6] D. Parkos, A. Alexeenko, M. Kulakhmetov, B. C. Johnson, and H. J. Melosh, Journal of Geophysical Research: Planets **120**, 2152–2168 (2015).

[7] A. Filippov and D. Rosner, International journal of heat and mass transfer **43**, 127–138 (2000).

[8] J.-P. M. Péraud and N. G. Hadjiconstantinou, Physical Review B **84**, p. 205331 (2011).

[9] G. Bird, The Physics of Fluids **6**, 1518–1519 (1963).

[10] G. C. Maitland and E. B. Smith, Journal of Chemical and Engineering Data **17**, 150–156 (1972).

[11] K. Koura, H. Matsumoto, and T. Shimada, Physics of Fluids A: Fluid Dynamics **3**, 1835–1837 (1991).

[12] K. Koura and H. Matsumoto, Physics of fluids A: fluid dynamics **3**, 2459–2465 (1991).

[13] A. Kersch, W. Morokoff, and C. Werner, Journal of applied physics **75**, 2278–2285 (1994).

[14] J. Fan, Physics of Fluids **14**, 4399–4405 (2002).

[15] A. L. Fetter and J. D. Walecka, *Theoretical Mechanics of Particles and Continua* (Dover Publications, 2012).

[16] I. Gamba, J. Haack, C. Hauck, and J. Hu, SIAM J. Sci. Comput. **39**, B658–B674 (2017).

[17] S. Jaiswal, A. Alexeenko, and J. Hu, Journal of Computational Physics **378**, 178–208 (2019).

[18] S. Jaiswal, J. Hu, and A. A. Alexeenko, "Fast Deterministic solution of the full Boltzmann equation on Graphics Processing Units," in *Proceedings of 31st Rarefied Gas Dynamics Symposium* (AIP, 2018).

[19] S. Jaiswal, A. A. Alexeenko, and J. Hu, arXiv preprint arXiv:1903.03056 (2019).

[20] W. Wagner, Journal of Statistical Physics **66**, 1011–1044 (1992).

[21] A. Alexeenko and S. Gimelshein, in *The Handbook of Fluid Dynamics*, edited by R. Jonhson (CRC Press Boca Raton, FL, 2016), pp. 39:1–40.

[22] A. Venkattraman and A. A. Alexeenko, Physics of Fluids **24**, p. 027101 (2012).

[23] S. Chapman, T. G. Cowling, and D. Burnett, *The mathematical theory of non-uniform gases: an account of the kinetic theory of viscosity, thermal conduction and diffusion in gases* (Cambridge university press, 1990).

[24] A. B. Weaver, A. Venkattraman, and A. A. Alexeenko, Physics of Fluids **26**, p. 107102 (2014).

[25] A. B. Weaver, "Assessment of high-fidelity collision models in the direct simulation Monte Carlo method," Ph.D. thesis, Purdue University, West Lafayette 2015.

[26] J. Crank *et al.*, *The mathematics of diffusion* (Oxford university press, 1979).

[27] M. A. Gallis, J. R. Torczynski, S. J. Plimpton, D. J. Rader, T. Koehler, and J. Fan, "Direct simulation Monte Carlo: The quest for speed," in *AIP Conference Proceedings*, Vol. 1628 (AIP, 2014), pp. 27–36.

[28] M. A. Gallis, N. P. Bitter, T. P. Koehler, J. R. Torczynski, S. J. Plimpton, and G. Papadakis, *Physical Review Letters*, **118**, p. 064501 (2017).

[29] M. A. Gallis, T. P. Koehler, J. R. Torczynski, and S. J. Plimpton, *Physical Review Fluids*, **1**, p. 043403 (2016).

[30] C. Pekardan and A. Alexeenko, AIAA Journal 765–779 (2017).

[31] I. B. Sebastiao, L. Qiao, and A. A. Alexeenko, *Combustion and Flame*, **198**, 40–53 (2018).

[32] A. B. Weaver and A. A. Alexeenko, Journal of Physical and Chemical Reference Data **44**, p. 023103 (2015).